EPR approaches to heterogeneous catalysis. The chemistry of titanium in heterogeneous catalysts and photocatalysts

EPR Approaches to Heterogeneous Catalysis. The Chemistry of Titanium in Heterogeneous Catalysts and Photocatalysts.

Elena Morra, Elio Giamello, Mario Chiesa*

Dipartimento di Chimica, Università di Torino, Via Giuria, 7 10125-Torino, Italy

e-mail: mario.chiesa@unito.it

Abstract

Paramagnetic species are often involved in catalytic or photocatalytic reactions occurring at the solid-gas interface of heterogeneous catalysts. In this contribution we will provide an overview of the wealth and breadth of information that can be obtained from EPR in the characterization of paramagnetic species in such systems, illustrating the advantages that modern pulsed EPR methodologies can offer in monitoring the elementary processes occurring within the coordination sphere of surface transition-metal ions. To do so we selected three representative systems, where titanium ions in low oxidation state act as active catalytic sites, trying to outline the methodological approaches which characterize the application of EPR techniques and the questions that can be answered and addressed relative to the characterization of heterogeneous catalytic materials.

Introduction.

Heterogeneous catalysis is based on reactions occurring at specific sites, located on the surface or within the channels of high surface area polycrystalline materials. [1] Understanding the electronic, chemical and structural properties of such sites, their interaction with the surrounding matrix and their changes during a particular process is of paramount importance for the development of new catalytic systems, with maximized atom efficiencies, that are both versatile and robust for industrial manipulation. To this aim, increasingly intricate active sites are being designed and created, which deserve a meticulous understanding of their structure–property relationships. In the vast majority of heterogeneous catalysts, such understanding is far from trivial due to the heterogeneity of the support, the plurality and low concentration of the active surface sites, combined with difficulties in investigating the catalysts under reaction conditions. It is clear that only the combination of a range of physicochemical, operando, and spectroscopic characterization techniques, possibly

complemented with quantum chemical modelling, can lead to a proper understanding of the nature and structure of the catalytic sites and ultimately to the implementation of new catalysts by design. Among the vast arsenal of spectroscopic techniques used for interrogating heterogeneous catalysts, Electron Magnetic Resonance techniques can be of importance in obtaining a molecular level description of the structure and reactivity of paramagnetic species. Such species, characterized by the presence of at least one unpaired electron, are frequently encountered in catalytic systems either as active species or catalytic intermediates and are often associated to transition metal ions (TMI). Key to the catalytic importance of TMI is the presence of partially filled *d* shells, leading, when stabilized at solid surfaces, to species with unusual oxidation states and coordination numbers. The complex ligand structure that surrounds the catalyst's central active site has a great influence in controlling the activity, selectivity and specificity of the catalyst and even subtle changes in the first and following coordination spheres deserve a thorough investigation.[2]

If it can be proven that the paramagnetic species is of importance within the catalytic cycle, EPR techniques can then provide unique insights into the geometric and electronic structure, the interaction with the environment and the dynamical processes of such species.

The potential of EPR spectroscopy in the characterization of heterogeneous catalysts and surfaces in general was early recognized, [3,4,5,6,7] but this potential is nowadays enormously extended thanks to the availability of advanced pulse methods [8] and the implementation of *in situ* (*operando*) techniques.[9] Different EPR approaches can thus be taken for heterogeneous catalysts characterization, which range from the study of well defined model systems under ultra-high vacuum conditions [10] to real catalysts under *operando* conditions (high pressure – temperature conditions) [11],[12] to real or model catalysts (high surface area polycrystalline systems) under controlled (*ex-situ*) conditions [13] [14],[15]. This last approach bridges the gap between surface science and operando methods, providing very valuable information, in particular in term of the local structure and coordination chemistry of surface paramagnetic sites. Typical methodologies in this case include thermal treatments under controlled atmosphere, testing of the reactivity at the solid-gas interface by means of diamagnetic and paramagnetic (e.g. O_2, NO, NO_2) probe molecules and the use of isotopic enrichment. Moreover, the ex-situ approach allows for the use of high resolution pulse EPR techniques, which usually are carried out at low temperature. These high resolution techniques allow resolving weak magnetic interactions, not usually resolved in conventional CW EPR experiments. In particular, ENDOR and ESEEM techniques allow detecting the NMR transition frequencies of nuclei coupled to unpaired electrons, providing unique information in both the local

structure and the nature of the chemical bond between the metal centre and the surrounding ligands.

The aim of the present work is thus to describe the opportunities (and limitations) offered by the application of advanced EPR techniques in conjunction with surface chemistry methodologies, to study the molecular structure of transition metal ions and complexes relevant to heterogeneous catalysis. To do so, we will use the case of Ti^{3+} ions in different heterogeneous systems, illustrated in Figure 1, where titanium ions exert different functionalities.

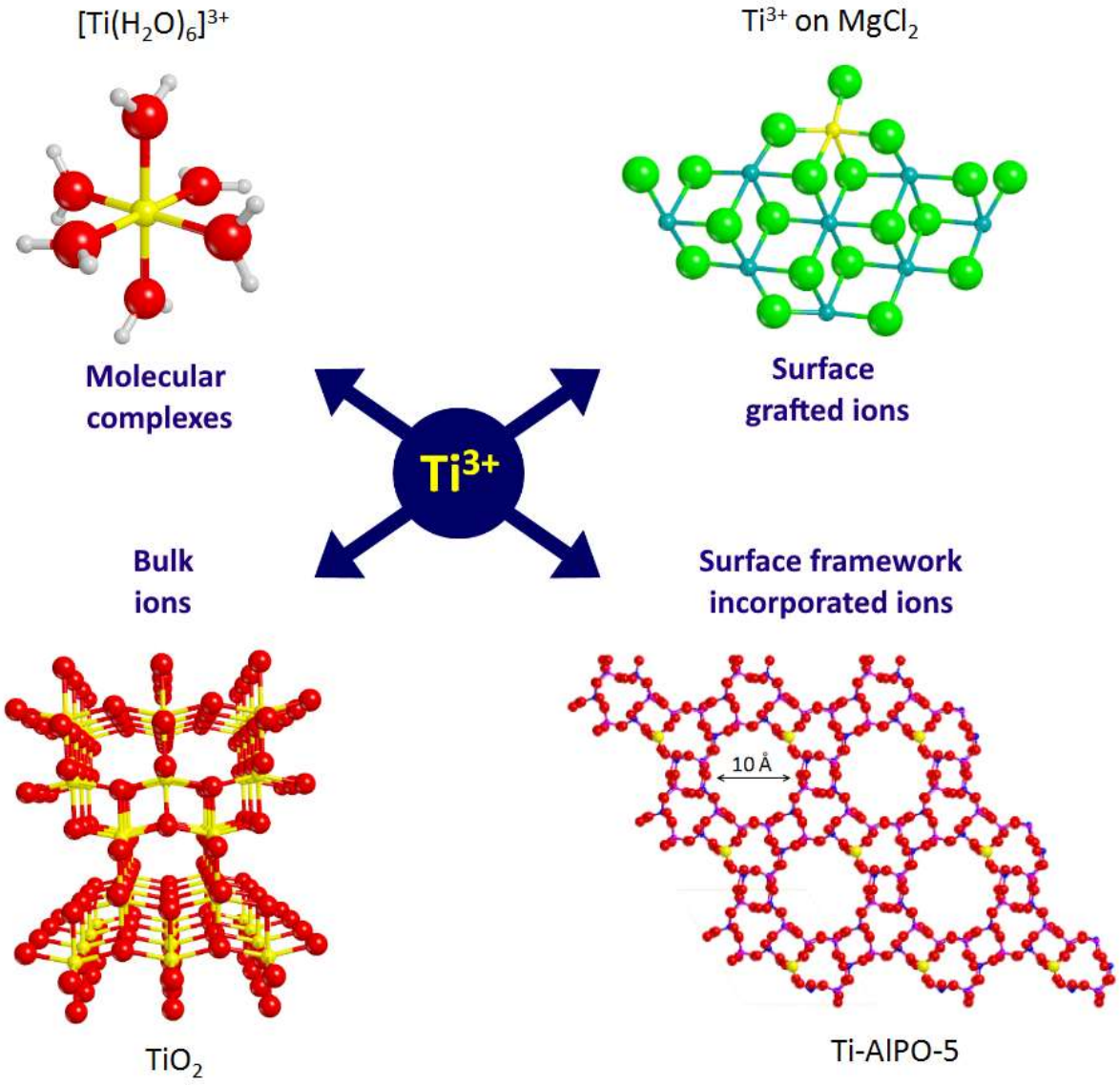

Figure 1 Ti ions in different environments treated in the text.

Titanium is the ninth most abundant element on Earth and is the second most abundant transition metal, after iron.[16] Titanium (III) and titanium (IV) are the most common oxidation states of this element, which features large in materials chemistry and catalysis. In the field of heterogeneous

catalysis, Ti-based catalysts have received much attention for their application in selective, catalytic oxidation of organic compounds[17-18,19] as well as in polymerization catalysis (Ziegler-Natta)[20,21] or photocatalysis.[22]

Highly-active and selective catalysts have been produced by dispersing titanium atomically in a silica matrix[23,24] or by grafting isolated titanium species to the surface of silica,[25-,26,27,28] mesoporous molecular sieves,[29-,30,31] layered aluminosilicates [32] or polyoxometallates.[33,34] Titanium-based microporous (e.g. titanosilicates such as TS-1 or aluminophosphate zeotype materials such as TiAlPOs)[35,36] and mesoporous solid (e.g. TiMCM-41)[37] materials have proven particularly effective in epoxidation reactions.

$MgCl_2$-supported $TiCl_4$ systems, where catalytically active species are generated by reductive activation with different alkylaluminium compounds are the basis of modern heterogeneous Ziegler-Natta catalysts, which are among the most effective and atom-economical catalysts available. Moreover, titanium dioxide (TiO_2) is one of the most investigated systems and can be considered as a model substrate to study phenomena concerned with photoelectric charge generation and transport, photocatalysis and water splitting.**Errore. Il segnalibro non è definito.**[38,39,40]

The high activity and selectivity of these different catalysts, is related to the local structural environment and coordination geometry, but also to the intrinsic nature of the metal ion site. In the following, EPR approaches and methodologies used in our laboratory to tackle these problems will be illustrated using the examples reported in Figure 1 as a guideline.

1. The EPR spectroscopy of Ti^{3+} – theoretical background

Ti^{3+} metal ions, by virtue of their $3d^1$ electronic configuration, are two level systems (S=1/2) representative of Kramer's doublet, which are degenerate in zero magnetic field and whose energy can be separated only by an applied magnetic field. Titanium ions in the 3+ oxidation state are therefore a paradigmatic example of transition metal ions of catalytic relevance whose chemistry can be directly and selectively investigated by means of EPR spectroscopy. [41-46]

In the case of titanium ions, the dominating interactions are the electron Zeeman interaction (characterized by the **g** matrix) and the hyperfine interactions of the unpaired electron with the isotopes ^{47}Ti (I=5/2, natural abundance 7.75%) and ^{49}Ti (I=7/2, natural abundance 5.51%). Due to the low natural abundance of the magnetically active isotopes however, the information derived from the CW EPR powder spectrum is usually limited to the electron Zeeman interaction, which is a useful reporter of the symmetry of the site. [47,48]

When Ti^{3+} is subjected to a perfect cubic crystalline field from tetrahedral or octahedral coordination, its 5-fold orbital degeneracy is split into two and three degenerate levels. In a tetrahedral field the doublet has lower energy, whereas in an octahedral field the reverse is true (Figure 2).

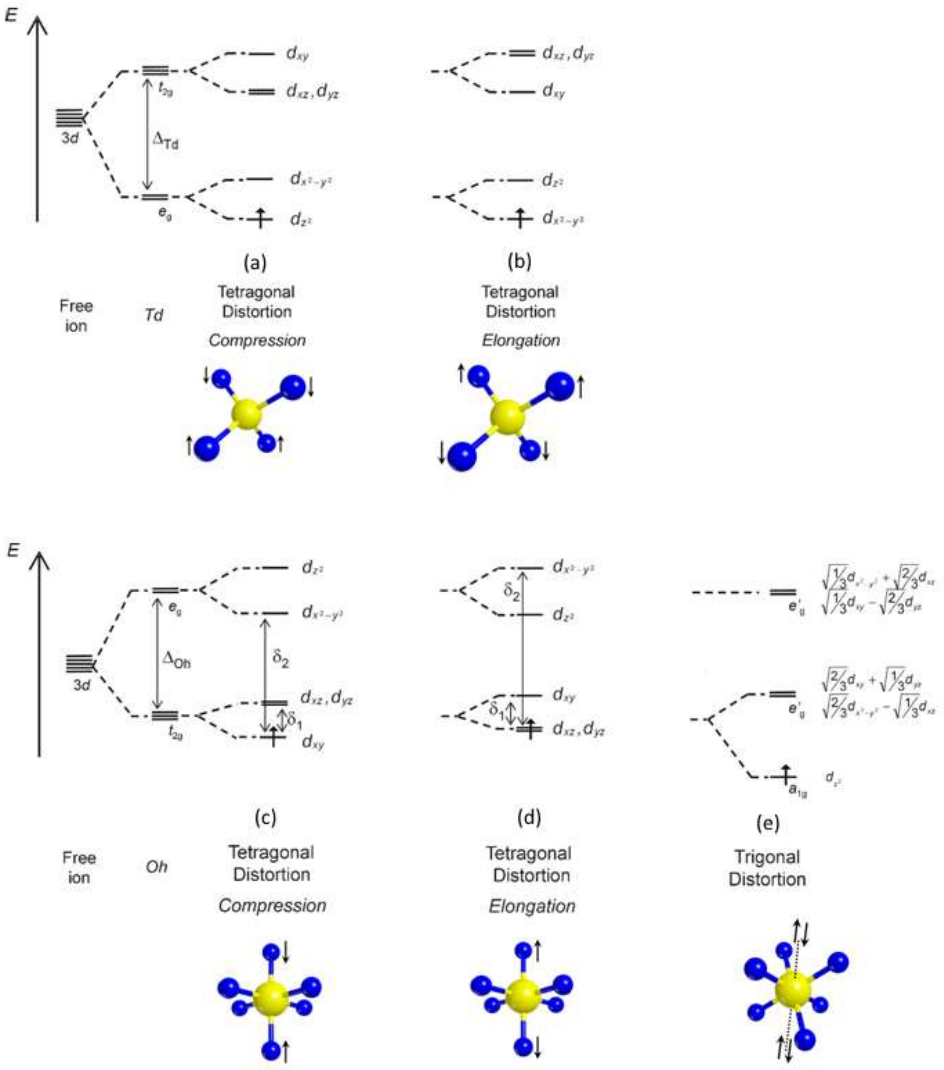

Figure 2. Level scheme for the *d*-orbitals of Ti^{3+} in a (a,b) tetragonal distorted tetrahedral crystal field, and in a (c,d) tetragonal or (e) trigonal distorted octahedral crystal field.

In the classical crystal-field theory, the EPR parameters are explained by using the perturbation formulas based on the one-spin-orbit (SO)-parameter model.[49] Under the effect of a tetrahedral crystal field the degenerate five *d* orbitals are split to give a doublet state and a triplet state as shown in Figure 2a,b. The effect of a further tetragonal distortion is shown in the case of both compression and elongation. If the tetragonal distortion is positive (tetragonal compression, Figure 2a), the d_{z^2} orbital lies lower in energy, while if the distortion is negative (tetragonal elongation,

Figure 2b), $d_{x^2-y^2}$ is the low-lying orbital. Considering the distortion axis along the *z*-direction, the *g* values are given, to first order, by the following equations in the case of tetragonal compression and elongation, respectively:

$$\boldsymbol{g_{\parallel} \cong g_e \text{ and } g_{\perp} \cong g_e - \frac{6\lambda}{\Delta_{Td}}} \quad (1)$$

$$\boldsymbol{g_{\parallel} \cong g_e - \frac{8\lambda}{\Delta_{Td}} \text{ and } g_{\perp} \cong g_e - \frac{2\lambda}{\Delta_{Td}}} \quad (2)$$

In Eq.1 and Eq.2 λ is the spin–orbit coupling constant (154 cm^{-1} for Ti^{3+}) and $\boldsymbol{\Delta_{Td}}$ is the energy separation between the degenerate triplet and doublet levels in the cubic tetrahedral field (Figure 2). Thus, for a tetragonal compression $\boldsymbol{g_{\perp} < g_{\parallel} \cong g_e}$ is expected, while for a tetragonal elongation $\boldsymbol{g_{\parallel} < g_{\perp} < g_e}$.

Typical values for Ti^{3+} subjected to a thetrahedrally distorted crystal field are reported in Table 1.

Centre	g_x	g_y	g_z	A_x	A_y	A_z	Ref.
Tetrahedral Sites							
Ti^{3+} Beryl	1.8656	1.9073	1.9880	Unres.	61	Unres.	[50]
Ti^{3+} Cordierite	1.9010	1.9135	1.9947	Unres.	64	Unres.	[50]
Ti^{3+} TS-1	1.922	1.939	1.9897	Unres.	Unres.	Unres.	[51]
Ti^{3+}AlPO	1.898	1.918	1.991	Unres.	Unres.	Unres.	[52]
Octahedral Sites Trigonal Distortion							
Ti^{3+} Beryl	1.8416	1.8416	1.9895	-6.0	-6.0	61	[50]
$Ti^{3+}(H_2O)_6$	1.896	1.896	1.994	Unres.	Unres.	Unres.	[53]

			Octahedral Sites Tetragonal Distortion				
Ti^{3+} rutile interstitial	1.9746	1.9780	1.9414	Unres.	Unres.	Unres.	[44]
Ti^{3+} rutile oxygen vacancy	1.9572	1.9187	1.8239	64.54	33.34	11.57	[54]
Ti3+ anatase (F-TiO2 powder)	1.99	1.99	1.96	Unres.	Unres.	Unres.	[55]

Table 1 Spin Hamiltonian parameters for Ti^{3+} in different coordination geometries. Hyperfine couplings are given in units of MHz.

When the metal ion is octahedrally coordinated, the free-ion ground state is split so to give a triplet state t_{2g} as the ground state (Figure 2). An additional tetragonal (Figure 2c,d) or trigonal (Figure 2e) distortion further lifts the degeneracy of the doublet and triplet levels and results in anisotropic *g* values. In the tetragonal case (D_{4h}), if the distortion is a tetragonal compression, the ground state is the d_{xy} orbital (Figure 2c), while if the distortion is tetragonal elongation (Figure 2d), the ground state is a degenerate d_{xy}, d_{yz} orbital. In the latter case, Ti^{3+} exhibits a Jahn-Teller effect that further resolves the degeneration. (The study of the influence of Jahn-Teller coupling in the case of Ti(III) containing compounds is vast and will not be dealt with here. The reader is referred to specific articles dealing with the subject[56,57,58,59]) The *g* value expressions for a Ti^{3+} ion in a tetragonally distorted octahedral environment are:

$$\boldsymbol{g_{\parallel} \cong g_e - \frac{8\lambda}{\delta_2}\ and\ g_{\perp} \cong g_e - \frac{2\lambda}{\delta_1}} \quad (3)$$

where δ_1 and δ_2 are the energy separation between the *d*-orbitals shown in Figure 2c,d.

In the case of trigonally distorted octahedral (D_{3d}) symmetry the five orbitals are split into three energy states, as shown in Figure 2e. The resulting *d* orbitals are quantized with respect to the three-fold axis, and the unpaired electron dwells in the d_{z^2} orbital. The calculated *g* values are analogous to those found for the tetragonally compressed tetrahedral symmetry (Eq.1):

$$\boldsymbol{g_{\parallel} \cong g_e\ and\ g_{\perp} \cong g_e - \frac{2\lambda}{\delta}} \quad (4)$$

Although CW-EPR can provide evidence for the local symmetry adopted by Ti^{3+} ions, the details of the ~~metal to ligand~~ interaction and the coordination geometry of first and second shells remain

largely undetermined. These interactions provide crucial details on the local structure of the paramagnetic species and on the nature of the chemical bond, allowing to provide a detailed description of those features of the molecular structure, related to the unpaired electron wave function distribution.

Pulse EPR methods, like HYSCORE and pulse ENDOR, allow the identification and investigation of the hyperfine and nuclear quadrupole interactions of the magnetic ligand nuclei (e.g. ^{1}H, ^{14}N, ^{27}Al, ^{31}P,^{13}C, ^{17}O …). HYSCORE spectroscopy [60] is a two-dimensional (2D) experiment in which a mixing pulse creates correlations between the nuclear frequencies in two different electron spin (m_S) manifolds. In this way NMR transitions of magnetically active nuclei in the surrounding of the paramagnetic species can be detected, coupling the sensitivity of EPR to the resolution of NMR.

In the following the wealth of information concerning structural features and chemical reactivity relevant to catalytic systems will be illustrated.

2. Ti ions in open framework systems. Structure and reactivity of tetra coordinated Ti^{3+} ions

The open-structure aluminosilicates (embracing natural and synthetic zeolites) as well as open-structure aluminophosphates (AlPOs), are prime examples of uniform heterogeneous catalysts. The incorporation of TMI in the open framework of these structures allows designing catalysts with specific functionalities and selectivities. Titanium insertion in tetrahedral sites of silicalite or of AlPO materials has been found particularly effective in enabling catalysts with superior conversions and selectivities in many important reactions,[36,61,62,63,64,65] the catalytic activity being associated to the coordinatively unsaturated tetrahedral Ti^{4+} ions.[64,66,67,68,69] One of the key aspects to be elucidated in the characterization of these materials is the exact location of the TMI, as most spectroscopic evidence for framework substitution is often indirect. EPR techniques can provide unambiguous and direct evidence concerning the location of a paramagnetic metal centre and allow following its coordination chemistry and chemical reactivity. To exemplify this case we show the results relative to the TiAlPO-5 system. Aluminophosphates AlPO-*n*, where *n* denotes a particular structure type, form a class of microporous crystalline materials comparable to the well-known zeolites and characterized by neutral lattices constituted by alternating PO_4 and AlO_4 tetrahedra (Figure 4).[70] AlPOs represent thus a class of open framework materials where isolated tetrahedral Ti sites can be obtained through isomorphous substitution and which are particularly interesting due to their specific activity towards different chemical processes. [65,71]

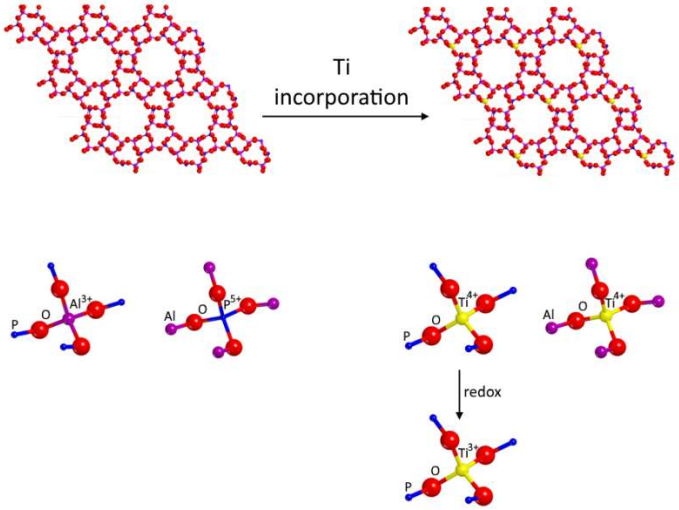

Figure 4 AlPO-5 framework structure and sites for titanium incorporation. See text for explanation.

Titanium incorporation into the aluminophosphate structure is of crucial importance in order to achieve significant catalytic performances, but actual incorporation into the tetrahedral framework is difficult to prove. Direct spectroscopic evidence can be obtained using CW-EPR and ~~Hyperfine Sublevel Correlation (~~HYSCORE~~)~~ spectroscopies, exploiting reduced Ti^{3+} centres as reportes.[52] It should be emphasized~~,~~ that the reduction of Ti^{4+} lattice ions to Ti^{3+} paramagnetic species~~,~~ is not only functional to the spectroscopic study, but offers the possibility to follow the redox chemistry of titanium in this specific system. The oxidation-reduction behaviour of TiAlPO represents an important issue, which can be tackled in a detailed way by means of EPR spectroscopy. In fact, while Ti^{4+} ions are EPR silent, Ti^{3+} is characterized by a d^1 electron configuration (S=1/2) and characteristic CW-EPR spectra, whose features strongly depend on the cation local symmetry (see section 2). Moreover, in the case of AlPO materials, the paramagnetic species (Ti^{3+}) is surrounded in its second coordination sphere, by distinct magnetically active nuclei: ^{31}P (I=1/2) and ^{27}Al (I=5/2) (Figure 4). The combination of conventional CW-EPR and HYSCORE spectroscopy allows to probe in detail the environment of Ti^{3+} ions. The CW-EPR spectrum of reduced TiAlPO-5 is dominated by an S=1/2 species with a nearly axial **g** tensor (Figure 5 spectrum *a* in the top left corner). The *g* values are typical for Ti^{3+} in a tetrahedral crystal field (see table 1) and the assignment is corroborated by the appearance of a broad band centred around 870 nm in the corresponding UV-Vis spectrum (Figure 5 spectrum *a* in the bottom left corner), characteristic of ligand field *d-d* transition of Ti^{3+} sites in *Td* coordination. This spectral feature, representing one of the very few examples of electronic spectra of Ti^{3+} ions in tetrahedral symmetry, is in good agreement with the expected 10*Dq* value on the basis of crystal field theory.**Errore. Il segnalibro non è definito.**[47,72] Analysis of the EPR and UV-Vis spectra

thus provides convincing evidence that upon reduction, isolated Ti^{3+} ions occupy a framework position, but at what site is titanium being substituted? This question can be answered by means of HYSCORE, which allows detecting the hyperfine interaction to the second ligand shell (^{27}Al and ^{31}P). A typical HYSCORE spectrum is shown in Figure 5 (spectrum a, in the left hand side panel) and contains different pairs of cross peaks indicated with P(1)-P(4) which stem from the superhyperfine interaction between the unpaired electron of Ti^{3+} and different ^{31}P nuclei. In the (+,+) quadrant a diagonal peak centred at the ^{27}Al nuclear Larmor frequency ($\nu_{(^{27}Al)}$ = 4.02 MHz) is also present, which is due to remote (matrix) ^{27}Al nuclei. The presence of large ^{31}P couplings typical for phosphate coordination, combined with the absence of such a coupling due to ^{27}Al, provides thus a unique and direct proof for framework substitution of Ti^{3+} for the isovalent Al^{3+}.

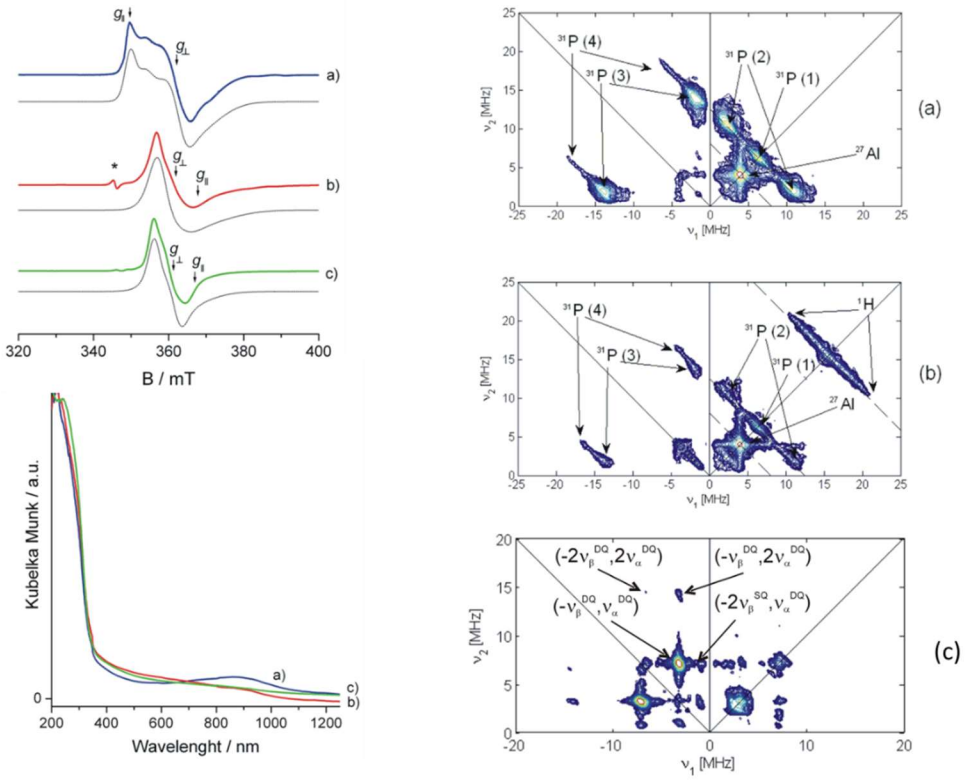

Figure 5 Top left: CW EPR spectra of a) Ti^{3+} ions in the AlPO-5 framework; b) spectrum recorded upon the adsorption of H_2O molecules; c) spectrum recorded upon the adsorption of NH_3 molecules. Bottom left: UV-Vis spectra recorded for the same samples. Right panel: HYSCORE spectra of a) Ti^{3+} ions in the AlPO-5 framework; b) upon H_2O adsorption; c) upon NH_3 adsorption.

After having elucidated the nature and location of the redox active titanium species, a very important question relative to the catalytic activity, is to assess their chemical accessibility and binding properties. This can be done by the adsorption of different probe molecules, which will bind to the Ti^{3+} sites modifying its coordination environment. This modification will be reflected by changes in the CW EPR spectrum and further details on the coordination geometry will be obtained

by the analysis of HYSCORE spectra. The coordination of water and ammonia molecules was used to this purpose. Upon water adsorption a new CW-EPR spectrum is observed (Figure 5 spectrum b in the top left corner) characterized by a different **g** tensor, typical of Ti^{3+} in distorted octahedral symmetry. A similar change is observed in the case of ammonia adsorption (Figure 5 spectrum c). Consistently with the modification of the EPR spectra, the *d-d* band at 870 nm is progressively depleted upon gas adsorption and a broad component at higher frequency emerges (Figure 5 bottom left corner spectra b and c). **Errore. Il segnalibro non è definito.** This shift is in agreement with the change in the **g** tensor of the EPR spectrum and consistent with an increase in the crystal field strength, suggesting that both H_2O and NH_3 molecules are entering in the coordination sphere of framework Ti^{3+} ions, as in octahedral $[Ti(H_2O)_6]^{3+}$ complexes, which are characterized by weak bands centred at 500 nm. The change from tetra to exa-coordination is also consistent with the decrease in the intensity of the *d-d* bands due to the presence of an inversion centre for octahedral coordination. The most direct evidence for molecular coordination comes however from HYSCORE spectroscopy (Figure 5 spectra b and c in the right hand side panel). Upon water coordination the HYSCORE spectrum is characterized by the presence of a proton ridge signal, with maximum extension of about 11 MHz. This ^{1}H coupling ~~correlates~~ with water proton couplings for the $[Ti(H_2O)_6]^{3+}$ model system[53] and unequivocally proves that the framework Ti^{3+} ions are chemically accessible and potentially reactive sites. In a similar way the HYSCORE spectra recorded upon ammonia adsorption are potent reporters of ammonia coordination through distinct ^{14}N couplings in the (-,+) quadrant. The spectra are dominated in the (−, +) quadrant by a pair of intense cross-peaks due to the double-quantum transitions (DQ) arising from the hyperfine interaction of the unpaired electron with a nitrogen nucleus (I = 1). Moreover, correlation peaks at ($-2\nu_\beta^{DQ}$, $2\nu_\alpha^{DQ}$) are observed, indicating that at least two virtually equivalent nitrogens, or in other words, at least two NH_3 molecules are binding to Ti^{3+} ions. This observation is particularly important in the context of understanding catalytic paths of reaction as identifying the number of coordinating molecules, provides crucial inputs for theoretical estimates of efficiency and kinetics of reactions.

A very interesting case, as a complement to the previous examples, is the coordination of ethylene due to the role played by open shell Ti^{3+} compounds in catalytic processes involving olefins polymerization such as in Ziegler Natta catalysis. The coordination of ethylene is the first step in the polymerization reaction, however experimental data relative to the $\{Ti^{3+}–C_2H_4\}$ due to the extreme reactivity of real catalysts are still missing. Isolated titanium ions in the AlPO matrix provide a nice model system to probe this interaction as the reactivity is strongly inhibited, allowing to isolate and

study the molecular complex. The combination of ^{1}H HYSCORE and SMART HYSCORE and ^{13}C HYSCORE experiments, in conjunction with DFT calculations provides a detailed description of the coordination of ethylene to Ti^{3+} ions, allowing to quantitatively assess the metal-to-substrate π*-back donation.

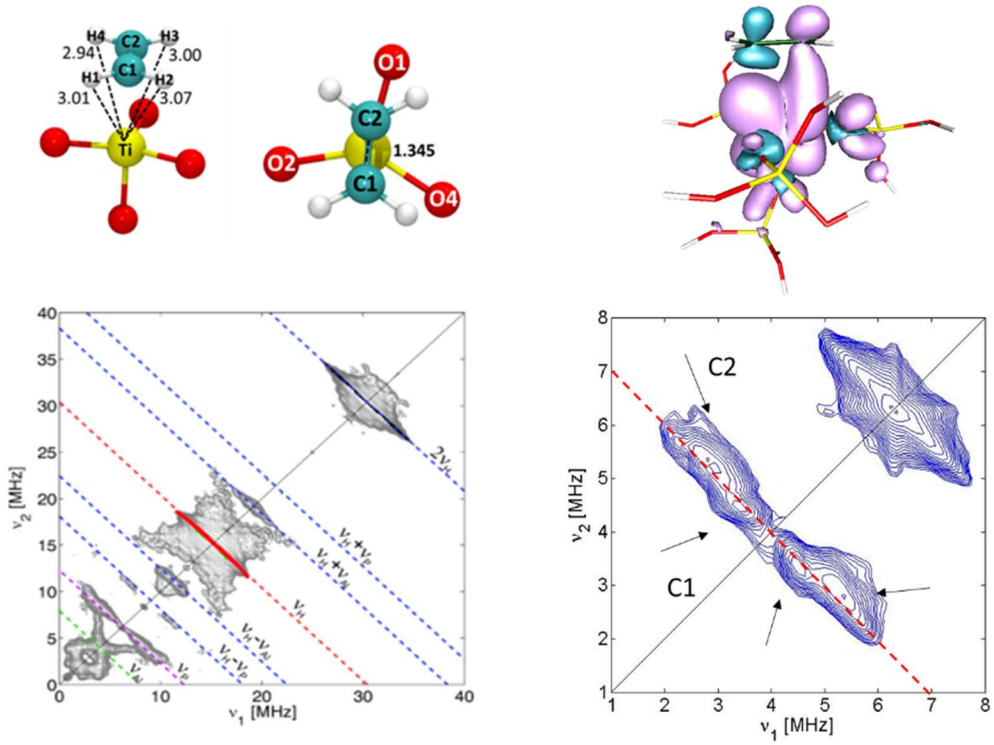

Figure 6 Top: DFT geometrical structure and spin density plot for ethylene coordination at Ti^{3+} framework sites of TiAlPO-5. Bottom left, ^{1}H SMART HYSCORE spectrum; bottom right ^{13}C HYSCORE spectrum.

Ethylene coordinates to Ti^{3+} ions via a classical donor-acceptor scheme typical for π coordination of olefins. Clearly, assessing the adsorption geometry is crucial in order to understand the nature of the chemical interaction and also to provide a guide for the DFT computations. A faithful descriptor of the adsorption geometry is provided by the proton hyperfine couplings. However, the HYSCORE ridges do not allow for the determination of the number of equivalent coupled protons, their tensors and their relative sign and orientations, which are crucial to establish the magnetic equivalence and the adsorption geometry. This important information can be at least partially obtained by the analysis of the DQ ridges, observed in Single MAtched Resonance Transfer (SMART) HYSCORE experiments.[73,74] The analysis of the ^{1}H SMART HYSCORE spectra provides evidence for the presence of at least two sets of magnetically equivalent protons, with different relative orientations. Comparison of the experimental values with those obtained from DFT computations reveals a good matching, validating the DFT optimized adsorption geometry. Key insights into the nature of the

chemical bond can then be obtained by ^{13}C HYSCORE experiments. Despite the sideon symmetry of the ethylene complex, the HYSCORE spectra reveal a clear asymmetry in the spin density distribution (Figure 6 bottom right) revealing the interesting structural feature of potential and actual inequality in the electronic spin states (α,β) on the two ethylene carbon atoms of the π coordinated ethylene molecule. This interesting feature is supported by DFT calculations, which cast the role of the oxygen donor ligand (O1 in Figure 6 top) in driving this bonding asymmetry.

These results bring into prominence the impact of electronic effects associated to the presence of singly occupied molecular orbitals, which has been so far disregarded in the field of olefin polymerization where, however, TMI in paramagnetic states feature large. In these reactions intermediate bond breaking, and further bond making is involved and the spin state of the reactant may have an important effect in directing the stereoselectivity of the catalyst.

Moving from this model study, in the next section we will show how this approach can lead to a molecular level understanding of putative active sites in a real, industrial Ziegler Natta catalyst for olefin polymerization.

Ti ions on $MgCl_2$ surfaces – Ziegler Natta Catalysts

Ziegler–Natta olefin polymerization is probably the most effective and atom-economical large-volume industrial chemical process and an almost unique example in chemistry of a development that arose from the synergy between fundamental research and industrial development. Sixty years after the discovery of the Ziegler catalyst however a molecular level description of the heterogeneous catalyst is still missing. Important advances in the understanding of this system have been ~~done~~ in the recent past in particular by approaching the problem from a basic point of view, employing for example the advanced techniques of surface science on various model systems, including the use of EPR under high vacuum conditions.[10] These approaches have led to singular advancements in the understanding of some specific problems; however no real attempt has been ~~done~~ so far to pursue a molecular level understanding of the role of paramagnetic species in real working catalysts. Our attempt [13] towards this goal was based on the combination of multifrequency (X, Q and W band) CW and pulse EPR techniques, the use of probe molecules and DFT modelling. An industrial ~~Ziegler Natta~~ catalyst was activated *in situ* with alkylaluminium vapours, leading to characteristic EPR spectra reported in Figure 7. The analysis of the spectra taken at different frequencies indicates that two EPR active Ti^{3+} species are predominant, indicating two distinct surface sites. Importantly, despite this is a real high surface area catalyst, the spectra are extremely

well defined as revealed by the absence of strain even in the ~~W band CW EPR~~ spectrum. This clearly indicates a high homogeneity of the Ti^{3+} species.

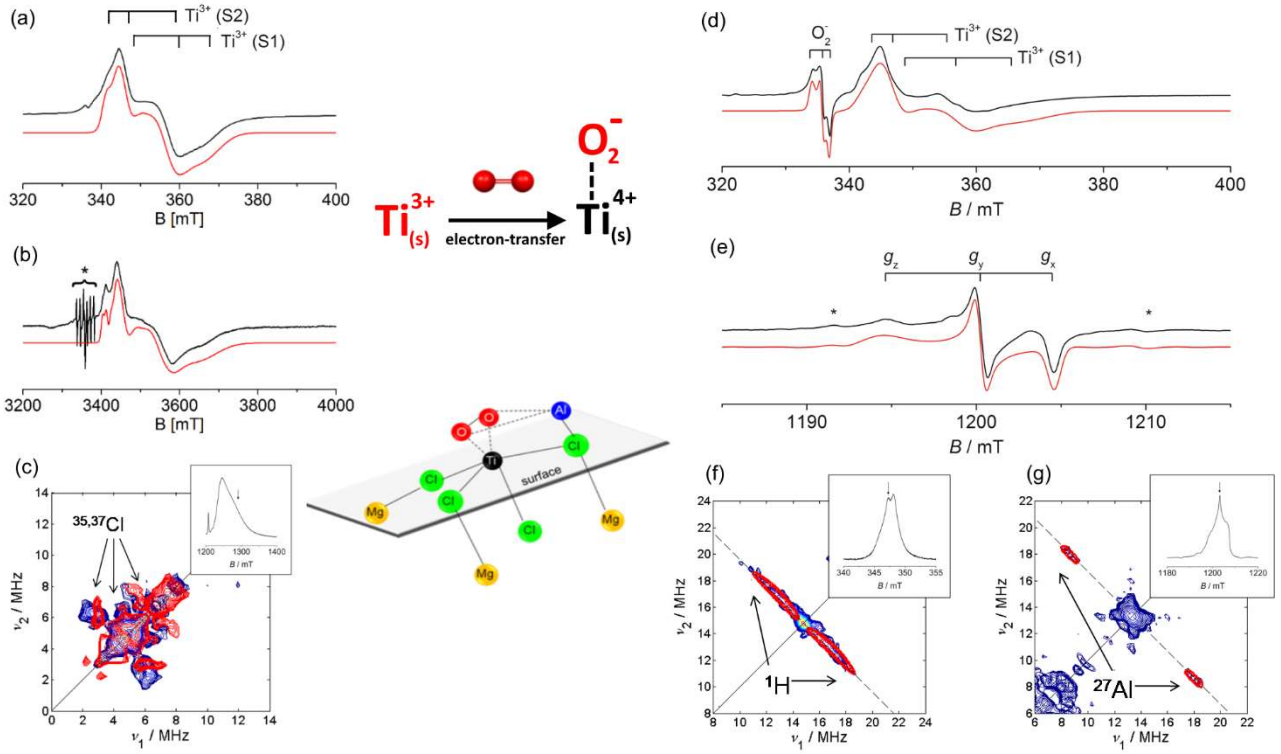

Figure 7 a) ~~X band~~ CW EPR b) ~~W band CW EPR~~ spectra of the activated catalyst; c) Q-band HYSCORE of the activated catalyst; d) ~~X band~~ CW EPR e) ~~Q band CW EPR~~ spectra recorded upon reaction of the activated catalyst; f) ~~X band~~ HYSCORE spectrum, g) ~~Q band~~ HYSCORE spectrum of the superoxide ion obtained upon reaction.

A combination of ~~Q band~~ HYSCORE and ~~W band ELDOR Detected~~ NMR spectra allowed to extract the hyperfine and nuclear quadrupole coupling tensors of coordinated chlorine ions. The spin Hamiltonian parameters are in good agreement with $TiCl_3$ molecular complexes [75] reinforcing the notion that these surface species can be regarded as well-defined single sites "solvated" on the support. The chemical reactivity and accessibility was then proven by reacting the sample with molecular oxygen. In this way superoxide anions are formed, which can then be further exploited as paramagnetic probes, revealing further details on the local environment of the adsorption site. In this way, evidence was obtained for the first time, for the presence of co-catalyst $Al(C_2H_5)_3$ residues in the proximity of the Ti^{3+} through distinct ^{27}Al hyperfine couplings (Figure 7g bottom right). This demonstrates that advanced EPR techniques can be applied to real working catalysts, providing a molecular level description of the active sites.

Ti ions in TiO_2 photocatalysts

An important aspect of the chemistry of low valence states of titanium is concerned with photo-catalytic reactions occurring on the surface of titanium dioxide (TiO_2). Titanium dioxide or titania is one of the most important binary metal oxides because of its extensive use as a white pigment and, more interestingly, because ~~its role of~~ sophisticated functional material in various photochemical and photophysical applications. The enormous attention devoted to titanium dioxide in the past few decades started with the discovery, at the beginning of the 1970's, of the photo-assisted water electrolysis performed in an electrochemical cell having a TiO_2 photoanode [38]. This experiment is usually considered as the starting point of the research that led to the development of both photocatalysis and artificial photosynthesis which are prominent fields of modern research. Later, titanium dioxide found another important application as a basic component of the third generation photovoltaic solar cells based on the dye sensitization of the oxide [76].

The photophysical properties of titanium dioxide are based on the process of light-induced charge separation that involves the promotion of an electron from the valence band to the conduction band of the oxide with consequent formation of an electron-hole pair.

$$TiO_2 + h\nu \rightarrow e^-_{(CB)} + h^+_{(VB)} \quad (5)$$

Both charge carriers (if they do not recombine) can be trapped at surface or bulk position of the solid. Holes are trapped by oxygen anions while electrons are trapped by cations thereby forming Ti^{3+} ions.

$$O^{2-} + h^+ \rightarrow O^- \quad (6)$$

$$Ti^{4+} + e^- \rightarrow Ti^{3+} \quad (7)$$

The surface trapped charge carriers possess a high chemical potential making them capable of entailing redox reactions with molecules present at the solid-liquid (or solid-gas) interface. The process of photocatalysis is indeed based on the reductive potential of photo-excited electrons and on the oxidative potential of the holes. The nature, location and properties of trapped charge carriers are therefore arguments of fundamental importance to understand the intimate mechanism of photocatalytic phenomena involving titanium dioxide and other semiconducting systems and it is not surprising that these properties have been the object of active research in past few decades (Ref 77 and references therein).

The contributions of electron magnetic resonance techniques to this field are based on the fact that the process of charge separation causes the formation of two separated paramagnetic entities. When stabilized by the solid matrix, both the trapped electron and the trapped hole are observed by EPR in terms of Ti^{3+} and O^- ions respectively as first shown by the experiment of Howe and Graetzel in 1985. [78]

The EPR spectroscopy of trivalent titanium ions in polycrystalline titanium dioxide was limited for many years to the analysis of the EPR signals monitored by the continuous wave (CW) technique. Information about the features of these ions was uniquely based on the structure of the **g** tensor since the low abundance of the two Ti isotopes having ~~non zero~~ nuclear spin (^{47}Ti, ^{49}Ti, see before) prevents the observation of the hyperfine structure of the signal in polycrystalline materials. The important information about the interaction of the unpaired *d*-electron of Ti^{3+} with its own nucleus, essential to have an idea about the degree of localization (or delocalization) of the trapped electron, is not therefore achievable by simple CW-EPR. The most important recent achievements obtained by means of CW-EPR about the properties of Ti^{3+} concern the rationalization of the *g* values of this species present in the various polymorphs of titania. These data that were obtained by systematic studies comparing experiments of controlled annealing, electron injection, chemical doping and photo-activation of the various solids [79, 80, 81] have led to a rationalization of the rather blurred picture resulting from various decades of experimental research mainly focused to the mere detection of the electron trapping centres rather than to their detailed physical description. The **g** tensor parameters of the most important Ti^{3+} centres due to isolated ions in the various matrixes are reported in Table 1, while for a general description of this topic the reader is referred to a specific review paper[82].

Polymorph	**Trapping site**	**g Matrix**		
		g_1	g_2	g_3
Anatase	Regular lattice site	1.992	1.992	1.962
	Surface sites (disordered environment)	g_{av} = 1.93		
Rutile	Regular lattice site	1.969	1.960	1.949
	Interstitial lattice site	1.9787	1.9750	1.9424
Brookite	Bulk lattice site	1.989	1.989	1.960
	Surface sites	1.939	1.929	1.893

Table 2. **g** tensor values of the main electron trapping sites in titanium dioxide polymorphs.

In this context advanced electron magnetic resonance technique, recently applied to the study of paramagnetic Ti centres in TiO_2, have allowed new insights into these systems mainly under two important points of view, the topological structure of the Ti^{3+} centers (surface or bulk)[79,83] and the degree of electron localization.[84]

To investigate both these aspects we introduced some years ago [85,86] a specific approach, consisting in the enrichment of the solid with ^{17}O (I = 5/2). According to the experimental procedure, ^{17}O enrichment in TiO_2 can be limited to the surface and subsurface layers or performed homogeneously into the whole solid as illustrated in Scheme 1.

a) Isotopic enrichment via gas-phase reactions (surface)

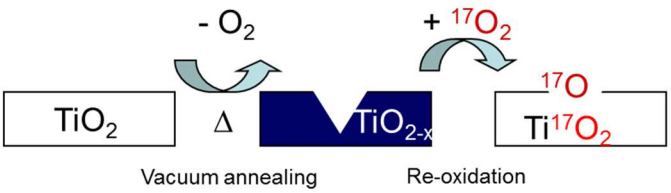

b) Isotopic enrichment via wet methods (bulk)

$$2\ H_2{}^{17}O + TiCl_4 \longrightarrow Ti^{17}O_2 + 4\ HCl$$

Scheme 1 Schematic illustration of ^{17}O enrichment methods used for surface and bulk enrichment of reducible oxides.

In the former case the propensity of TiO_2 – a reducible oxide – to release oxygen from the lattice in an oxygen-poor atmosphere is exploited. Upon annealing under vacuum oxygen vacancies are generated, with the formation of charge compensating Ti^{3+} ions, according to the following equation:

$$O^{2-} + 2Ti^{4+} \rightarrow \tfrac{1}{2}\ O_2 + V_O^{\bullet\bullet} + 2Ti^{4+} + 2e^- \rightarrow \tfrac{1}{2}\ O_2 + V_O^{\bullet\bullet} + 2Ti^{3+} \quad (8)$$

where the Kröger-Vink notation for defects (oxygen vacancy) is adopted. The reduced solid is then re-oxidized under $^{17}O_2$ at the same temperature of annealing (usually 773K). The oxygen vacancies, more abundant at the surface and in the immediate subsurface layers, are therefore filled with the magnetic oxygen isotope, leading to surface enriched samples:

$$\tfrac{1}{2}\ {}^{17}O_2 + V_O^{\bullet\bullet} + 2Ti^{3+} \rightarrow {}^{17}O^{2-} + 2Ti^{4+} \quad (9)$$

On the other hand, homogeneous isotopic enrichment of titanium dioxide powders is obtained by wet chemical methods using ^{17}O enriched water ($H_2{}^{17}O$) to hydrolize $TiCl_4$:

$$2\ H_2{}^{17}O\ +\ TiCl_4 \rightarrow\ Ti^{17}O_2 +\ 4\ HCl \qquad (10)$$

The identification of the surface or bulk nature of charge separated states, is clearly important in the context of chemical reactivity and catalysis. While the distinction can in general be done by testing the chemical reactivity of a reduced sample towards adsorbed molecular species (e.g. O_2), in the case of semiconducting oxides such as TiO_2, this approach is not always successful due to easy bulk to surface charge migration. Hyperfine techniques clearly provide a way to explore the local environment of trapped electrons and holes by monitoring weak hyperfine interactions arising from the presence of nearby magnetically active nuclei. As an example 2-pulse ESEEM experiments have been used to prove the surface nature of photogenerated holes in TiO_2 colloidal solutions, through the detection of remote ^1H hyperfine couplings.[83] In this context, isotopically enriched surfaces can provide very useful in understanding the topological features of Ti^{3+} centres obtained by different reduction methods, which in turn is of fundamental importance to understand the catalytic activity of a material. The reduction of TiO_2 anatase leads to two main EPR signal of Ti^{3+} whose ratio, in quantitative terms, depends on the method used for generating the centers. The former is a narrow axial signal with the main components at $g_{zz}= g_{\|}$=1.962 and $g_{xx}=g_{yy}=g_{\perp}$= 1.992 (species A) while the second one is a broad line centred at g_{av} = 1.93 (species B). Due to the broad line-width, this signal is best observed in Electron Spin Echo (ESE) detected experiments, which provide the absorption EPR spectrum (Figure 8a). The study of electron trapping Ti^{3+} centers in anatase was thus performed using ^{17}O surface enriched titanium dioxide (Scheme 1 a).

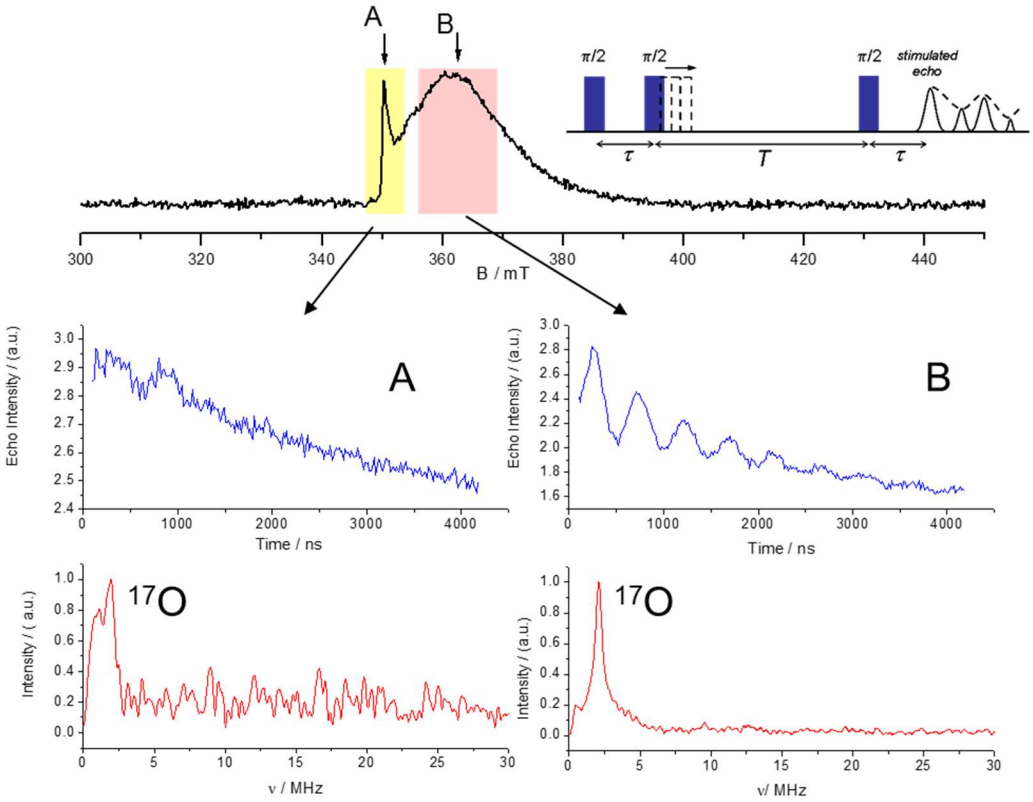

Figure 8 Top ESE detected EPR spectrum of Ti^{3+} centres in ^{17}O surface enriched anatase (*T*=10K); bottom, left hand-side time and frequency domain 3-pulse ESEEM spectra taken at observer position A; bottom, right hand-side corresponding spectra taken at observer position B.

The ^{17}O enriched sample was reduced by photoirradiating the anatase sample in the presence of molecular hydrogen. In this way only Ti^{3+} centres are formed, H_2 acting as an hole scavenger. The reaction clearly takes place at the gas-solid interface, and the two EPR signals, indicated with A and B in Figure 8 are observed in the ESE EPR spectrum. ~~3-Pulse~~ ESEEM spectra where then taken at magnetic field settings corresponding to species A and B respectively. **Errore. Il segnalibro non è definito.** The three-pulse ESEEM patterns shows an ^{17}O modulation depth which is rather strong in the case of species B (Figure 8 right hand-side), indicating a high number of ^{17}O nuclei interacting with the Ti^{3+} centres, and nearly absent in the case of species A (Figure 8 left hand-side). The corresponding Fourier transform spectra consist of a single sharp peak centred at about 2.1 MHz corresponding to the ^{17}O Larmor frequency. Since the ^{17}O enrichment is limited to the surface and subsurface region of the sample the result can be interpreted only assuming that the species corresponding to signal B is localized at the surface of the nanocrystals, while part of the excess electron charge migrates to the bulk giving rise to species A. The experiment described above provides an important methodological approach for the discrimination among the various electron

trapping centres at the surface of titanium dioxide distinguishing between bulk-located and surface-located sites. A word of caution should be injected at this stage, as care has to be taken in drawing conclusions when the expected signal is not observed in an ESEEM spectrum. Although the absence of the signal can be linked to a particular structural or topological characteristic, instrumental and technical reasons may also lie behind the missing signal. In these cases complementary experiments should always be performed.

Just as important as the topological structure is ~~the issue related to~~ the extent of localization of the unpaired electron wave function at the trapping titanium sites. The photophysical and photochemical properties of photoactive oxides are in fact strictly related to the motion of photogenerated charge carriers within the crystal and to their degree of localization at suitable sites of the solid. The case of trapped electrons in TiO_2 has been particularly discussed in the literature in the past two decades. As mentioned before an electron can be trapped by a Ti^{4+} site which formally becomes a Ti^{3+} ion. However, this simple chemical description is not sufficient to capture the nature that an electron trapped in a semiconducting oxide assumes, in particular in terms of localisation of the charge. An excess electron can be in principle fully localised onto the trapping ionic site thus constituting a self-trapped polaron [87] or in other cases can be delocalised over a group of ions belonging to a particular a region of the crystal (e.g. a row, a plane, or a given volume)[88] . Investigating the degree of localisation (or delocalisation) of a trapped charge is not an easy task using the available physical techniques and conflicting proposals are available in literature relative to the same kind of site.[89] If from the experimental side the situation is intricate~~d~~, theoretical calculations produce in some case conflicting results. These are related either to the computational approach adopted or, as recently shown in the case of trapped electrons in anatase, to the fact that computations find opposite solutions (localized/delocalized) having energy values very close one to the other thus preventing a clear indication. [90]

A clear-cut indication concerning the degree of localization of the unpaired electron wave function comes from the hyperfine interaction. Unfortunately the low natural abundance of magnetically active Ti isotopes, prevents the measurements of such interactions in polycrystalline TiO_2 samples. We found that ^{17}O enrichment provides a useful and relatively economical way around the problem. HYSCORE experiments were carried out on two different (homogeneously) ^{17}O enriched phases of titanium dioxide (Scheme 2 b), rutile and anatase. With this approach the hyperfine interactions of Ti^{3+} to the ^{17}O ligands were detected in the case of two specific centres, the regular site of anatase[79] and the interstitial Ti^{3+} site in rutile.[84] The obtained values can then be conveniently compared to

those observed and compared to those observed for the $[Ti(H_2{}^{17}O)_6]^{3-}$ molecular complex,[53] a genuinely, fully localized system.

The results are simply illustrated by Figure 9 where comparison is set to representative ^{17}O HYSCORE spectra recorded for the two different samples, namely a sub-stoichiometric rutile containing interstitial Ti^{3+} ions (g_1= 1.9787, g_2=1.9750, g_3= 1.9424) and an anatase sample containing excess electrons homogeneously diluted in the bulk and introduced via fluorine doping (signal A, g_{zz}= $g_{\parallel}$=1.962 and g_{xx}=g_{yy}=$g_{\perp}$= 1.992).

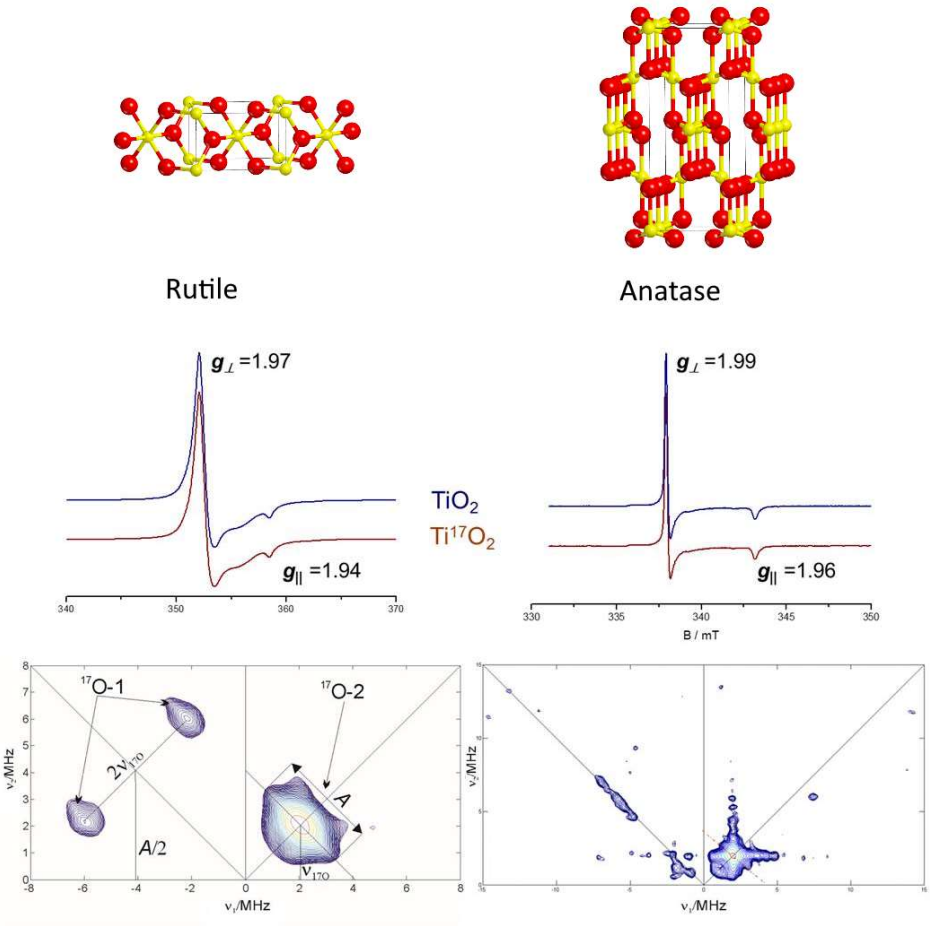

Figure 9. CW EPR and ^{17}O HYSCORE spectra of interstitial Ti^{3+} ions in rutile (left hand side) and Ti^{3+} ions in Fluorine doped anatase (right hand side).

The two HYSCORE spectra are characterized by the presence of peaks centred at the ^{17}O nuclear Larmor frequency, however the spectrum of the rutile sample shows two cross peaks in the (-,+) quadrant, which are absent in the spectrum of the anatase sample. Orientationally selected HYSCORE experiments allowed determining the full ^{17}O hyperfine tensor, which is dominated by an a_{iso} term of about 8 MHz. This value is fully comparable with the one observed for the $[Ti(H_2{}^{17}O)_6]^{3-}$ molecular complex, clearly proving that in this case the excess electron is fully localized on the titanium ion, which can indeed be regarded as a genuine Ti^{3+} ion. In the case of the anatase sample the cross peaks corresponding to the strong

hyperfine coupling are absent and a maximum coupling of 3 MHz is observed for this sample, which clearly indicates that in this case, a delocalized electron wave function samples a larger number of O lattice ions. These results, clearly show that in the two different polymorphs of TiO_2 – characterized by the same chemical composition but different crystal lattices – excess electrons display distinctly different behaviours with a clear propensity of rutile to localize excess electrons forming small polarons, while electrons in anatase "prefer a free-carrier state". These conclusions have been fully confirmed by STM studies and emphasize how even small structural variations in the lattice structure can lead to very different behaviour. [91]

The different charge trapping behaviour of the two main TiO_2 polymorphs, may be an important step towards the understanding of the amazing (and not yet explained) differences in the behaviour of rutile and anatase in photocatalytic reactions. In spite of the similarities of the two solids in terms of structural features, band gap values and flat band potentials the photocatalytic activity of anatase is in fact always higher than that of rutile.

Conclusions

A thorough understanding – at the molecular level – of structure-property relationships between catalytic active sites and the surrounding matrix, as well as with molecular adsorbates, is a necessary pre-requisite to rationally design new, more efficient catalysts. Among a vast range of physic chemical techniques, EPR can provide such a molecular level understanding, when paramagnetic species are concerned. We have illustrated the potential of EPR techniques, with emphasis on hyperfine techniques, to study the structure and reactivity of heterogeneous catalysts containing paramagnetic species. Examples, taken mainly from our laboratory, have been chosen to exemplify the breath of information that can be obtained as well as the methodological approach for the application of these techniques to the characterization of model and real heterogeneous catalysts. In particular, the role of hyperfine techniques in elucidating the nature and behaviour of catalytically active sites has been stressed together with the importance of coupling the EPR characterization with other experimental and theoretical techniques that can compensate for the intrinsic limitation of EPR, namely its restriction to paramagnetic species only. Using titanium as prototypical example of a transition metal ion, the role of CW EPR in probing the redox activity and coordination symmetry was shown. Hidden in the heterogeneously broadened EPR lines, a large amount of key information are present, arising from unresolved hyperfine couplings with surrounding magnetic nuclei. This information can be recovered by means of hyperfine techniques, which provide crucial insights into

the local environment and coordination chemistry of the paramagnetic species, allowing for a molecular level understanding of the geometric and electronic structure of paramagnetic catalytic sites.

References

[1]G. A. Somorjai, Introduction to surface chemistry and catalysis, Wiley, New York, (1994).

[2]K. Dyrek, M. Che, EPR as a tool to investigate the transition metal chemistry on oxide surfaces, Chem. Rev. 97 (1997) 305-332.

[3] F. Adrian, Guidelines for interpreting electron spin resonance spectra of paramagnetic species adsorbed on surfaces, J. Colloid Interf. Sci. 26 (1968) 317-354.

[4] J. H. Lunsford, Electron spin resonance in catalysis, Adv. Catal. 22 (1972) 265-344.

[5] M. Che, E. Giamello, Chapter 5: electron paramagnetic resonance, Stud. Surf. Sci. Catal. 12 (1990) B265-B332.

[6] R. F. Howe, Electron paramagnetic resonance spectroscopy of catalytic surfaces, Colloids Surf. A 72 (1993) 353–363.

[7] Z. Sojka, Molecular aspects of catalytic reactivity. Application of EPR spectroscopy to studies of the mechanism of heterogeneous catalytic reactions, Catal. Rev. Sci. Eng. 37 (1995) 461-512.

[8] D. Goldfarb, Electron Paramagnetic Resonance. A practitioner's toolkit. in: M. Brustolon, E. Giamello (Eds), J. Wiley and Sons, Hoboken (2009).

[9] A. Brukner, In situ electron paramagnetic resonance: a unique tool for analyzing structure–reactivity relationships in heterogeneous catalysis, Chem.Soc.Rev. 39 (2010) 4673-4684.

[10] T. Risse, J. Schmidt, H. Hamann, H.-J. Freund, Direct observation of radicals in the activation of Ziegler–Natta catalysts, Angew. Chem. Int. Ed. 41 (2002) 1517-1520.

[11] M. Brandhorst, S. Cristol, M. Capron, C. Dujardin, H. Vezin, G. Lebourdon, E. Payen, Catalytic oxidation of methanol on Mo/Al_2O_3 catalyst: An EPR and Raman/infrared operando spectroscopies study, Catalysis Today 113 (2006) 34-39.

[12] A. Brukner, Killing three birds with one stone – simultaneous operando EPR/UV-vis/Raman spectroscopy for monitoring catalytic reactions, Chem. Commun. 13 (2005) 1761-1763.

[13] E. Morra, E. Giamello, S. Van Doorslaer, G. Antinucci, M. D'Amore, V. Busico, M. Chiesa, Probing the coordinative unsaturation and local environment of Ti^{3+} sites in an activated high-yield Ziegler–Natta catalyst, Angew. Chem. Int. Ed. 54 (2015) 4857-4860.

[14] P. Pietrzyk, T. Mazur, K. Podolska-Serafin, M. Chiesa, Z. Sojka, Intimate binding mechanism and structure of trigonal nickel(I) monocarbonyl adducts in ZSM-5 zeolite - spectroscopic continuous wave EPR, HYSCORE, and IR studies refined with DFT quantification of disentangled electron and spin density redistributions along σ and π channels, J. Am. Chem. Soc. 135 (2013) 15467-15478.

[15] P. Schwach, M. Eichelbaum, R. Schlögl, T. Risse, K.-P. Dinse, Evidence for exchange coupled electrons and holes in MgO after oxidative activation of CH_4: a multifrequency transient nutation EPR study, J. Phys. Chem. C 120 (2016) 3781-3790.

[16]J. Emsley, The elements, 3rd ed., Clarendon Press, Oxford, (1998).

[17]I. W. C. E. Arends, R. A. Sheldon, M. Wallau, U. Schuchardt, Oxidative transformations of organic compounds mediated by redox molecular sieves, Angew. Chem. Int. Ed. 36 (1997) 1144-1163.

[18]R. A. Sheldon, Redox molecular sieves as heterogeneous catalysts for liquid phase oxidations, Stud. Surf. Sci. Catal. 110 (1997) 151-175.

[19]I. W. C. E. Arends, R. A. Sheldon, Activities and stabilities of heterogeneous catalysts in selective liquid phase oxidations: recent developments, Appl. Catal. A 212 (2001) 175-187.

[20]J. R. Severn, J. C. Chadwick, R. Duchateau, N. Friedrichs, Bound but not gagged – immobilizing single-site α-olefin polymerization catalysts, Chem. Rev. 105 (2005) 4073-4147.

[21]L. L. Böhm, The ethylene polymerization with Ziegler catalysts: fifty years after the discovery, Angew. Chem. Int. Ed. 42 (2003) 5010-5030.

[22]M. A. Henderson, A surface science perspective on TiO_2 photocatalysis, Surf. Sci. Rep. 66 (2011) 185-197.

[23]D. C. M. Dutoit, M. Schneider, A. Baiker, Titania-silica mixed oxides: I. Influence of sol-gel and drying conditions on structural properties, J. Catal. 153 (1995) 165-176.

[24]S. Klein, S. Thorimbert, W. F. Maier, Amorphous microporous titania–silica mixed oxides: preparation, characterization, and catalytic redox properties, J. Catal. 163 (1996) 476-488.

[25]E. Jorda, A. Tuel, R. Teissier, J. Kervennal, Synthesis, characterization, and activity in the epoxidation of cyclohexene with aqueous H_2O_2 of catalysts prepared by reaction of TiF_4 with silica, J. Catal. 175 (1998) 93-107.

[26]S. A. Holmes, F. Quignard, A. Choplin, R. Teissier, J. Kervennal, Tetraneopentyltitanium derived supported catalysts: Part 1. Synthesis and catalytic properties for the epoxidation of cyclohexene with aqueous hydrogen peroxide, J. Catal. 176 (1998) 173-181.

[27]J. M. Fraile, J. I. Garcia, J. A. Mayoral, E. Vispe, Silica-supported titanium derivatives as catalysts for the epoxidation of alkenes with hydrogen peroxide: A new way to tuneable catalytic activity through ligand exchange, J. Catal. 189 (2000) 40-51.

[28]E. Gianotti, C. Bisio, L. Marchese, M. Guidotti, N. Ravasio, P. Psaro, S. Coluccia, Ti(IV) catalytic centers grafted on different siliceous materials: spectroscopic and catalytic study, J. Phys. Chem. C 111 (2007) 5083-5089.

[29]T. Maschmeyer, F. Rey, G. Sankar, J. M. Thomas, Heterogeneous catalysts obtained by grafting metallocene complexes onto mesoporous silica, Nature 378 (1995) 159-162.

[30]S. Krijnen, B. L. Mojet, H. C. L. Abbenhuis, J. H. C. Van Hooff, R. A. Van Santen, MCM-41 heterogenised titanium silsesquioxane epoxidation catalysts: a spectroscopic investigation of the adsorption characteristics, Phys. Chem. Chem. Phys. 1 (1999) 361-365.

[31]W. Adam, A. Corma, H. Garcia, O. Weichold, Titanium-catalyzed heterogeneous oxidations of silanes, chiral allylic alcohols, 3-alkylcyclohexanes, and thianthrene 5-oxide: a comparison of the reactivities and selectivities for the large-pore zeolite Ti-β, the mesoporous Ti-MCM-41, and the layered alumosilicate Ti-ITQ-2, J. Catal. 196 (2000) 339-344.

[32]A. Corma, U. Diaz, V. Fornes, J. L. Jorda, M. Domine, F. Rey, Ti/ITQ-2, a new material highly active and selective for the epoxidation of olefins with organic hydroperoxides, Chem. Commun. (1999) 779-780.

[33]F. X. Gao, T. Yamase, H. Suzuki, H_2O_2-based epoxidation of bridged cyclic alkenes with $[P\{Ti(O_2)\}_2W_{10}O_{38}]^{7-}$ in monophasic systems: active site and kineticsJ. Mol. Catal. A: Chem. 180 (2002) 97-108.

[34]O. A. Kholdeeva, T. A. Trubitsina, R. I. Maksimovskaya, A. V. Golovin, W. A. Neiwert, B. A. Kolesov, X. Lopez, J. M. Poblet, First isolated active titanium peroxo complex: characterization and theoretical study, Inorg. Chem. 43 (2004) 2284-2292.

[35]G. Bellussi, A. Carati, G. M. Clerici, G. Maddinelli, R. Millini, Reactions of titanium silicalite with protic molecules and hydrogen peroxide, J. Catal. 133 (1992) 220-230.

[36]B. Notari, Microporous crystalline titanium silicates, Adv. Catal. 41 (1996) 253-334.

[37]P. T. Tanev, M. Chibwe, T. J. Pinnavaia, Titanium-containing mesoporous molecular sieves for catalytic oxidation of aromatic compounds, Nature 368 (1994) 321-323.

[38]A. Fujishima, K. Honda, Electrochemical photolysis of water at a semiconductor electrode, Nature 238 (1972) 37-38.

[39]M. Matsuoka, M. Kitano, M. Takeuchi, M. Anpo, J. M. Thomas, Photocatalytic water splitting on visible light-responsive TiO_2 thin films prepared by a RF magnetron sputtering deposition method, Top. Catal. 35 (2005) 305-310.

[40]U. Diebold, The surface science of titanium dioxide, Surf. Sci. Rep. 48 (2003) 53-229.

[41]D. Gourier, E. Samuel, Proton, titanium-47 and titanium-49 ENDOR study on frozen solutions of [(.eta.5-C5H5)Ti(.eta.8-C8H8)] and [(.eta.5-CH3C5H4)Ti(.eta.8-C8H8)], J. Am. Chem. Soc. 109 (1987) 4571-4578.

[42]M. Horáček, V. Kupfer, U. Thewalt, M. Polašek, K. Mach, Synthesis and structures of paramagnetic binuclear (η^8-1,4-bis(trimethylsilyl)cyclooctatetraenide)titanium(III) chlorides, J. Organomet. Chem. 579 (1999) 126-132.

[43]A. M. Prakash, L. Kevan, M. H. Zahedi-Niaki, S. Kaliaguine, Electron spin resonance and electron spin−echo modulation evidence for the isomorphous substitution of titanium in titanium aluminophosphate molecular sieves, J. Phys. Chem. B 103 (1999) 831-837.

[44]M. Aono, R. R. Hasiguti, Interaction and ordering of lattice defects in oxygen-deficient rutile TiO_{2-x}, Phys. Rev. B 48 (1993) 12406-12414.

[45]R. F. Howe, M. Grätzel, EPR observation of trapped electrons in colloidal titanium dioxide, J. Phys. Chem. 89 (1985) 4495-4499.

[46]S. Van Doorslaer, J. J. Shane, S. Stoll, A. Schweiger, M. Kranenburg, R. J. Meier, Continuous wave and pulse EPR as a tool for the characterization of monocyclopentadienyl Ti(III) catalysts, J. Organomet. Chem. 634 (2001) 185-192.

[47]B. N. Figgis, Introduction to Ligand Fields, John Wiley & Sons, New York (1967).

[48]J. A. Weil, J. R. Bolton, J. E. Wertz, Electron paramagnetic resonance: elementary theory and practical applications, John Wiley, New York (1994).

[49]A. Abraham, B. Bleaney, Electron paramagnetic resonance of transition ions, Oxford University Press, Oxford (1970).

[50]V. P. Solntsev, A. M. Yurkin, Valence states and coordination of titanium ions in beryl crystals, Cryst. Reports. 45 (2000) 128-132.

[51]E. Morra, E. Giamello, M. Chiesa, Probing the redox chemistry of titanium silicalite-1: formation of tetrahedral Ti^{3+} centers by reaction with triethylaluminum, Chem. Eur. J. 20 (2014) 7381-7388.

[52]S. Maurelli, V. Muthusamy, M. Chiesa, G. Berlier, S. Van Doorslaer, Elucidating the nature and reactivity of Ti ions incorporated in the framework of $AlPO_4$-5 molecular sieves. New evidence from ^{31}P HYSCORE spectroscopy, J. Am. Chem. Soc. 133 (2011) 7340-7343.

[53] S. Maurelli, S. Livraghi, M. Chiesa, E. Giamello, S. Van Doorslaer, C. Di Valentin, G. Pacchioni, Hydration structure of the Ti(III) cation as revealed by pulse EPR and DFT studies: new insights into a textbook case, Inorg. Chem. 50 (2011) 2385-2394.

[54]A. T. Brant, N. C. Giles, S. Yang, M. A. R. Sarker, S. Watauchi, M. Nagao, I. Tanaka, D. A. Tryk, A. Manivannan, L. E. Halliburton, Ground state of the singly ionized oxygen vacancy in rutile TiO_2, Appl. Phys. 114 (2013) 113702-113702-10.

[55] A. M. Czoska, S. Livraghi, M. Chiesa, E. Giamello, S. Agnoli, G. Granozzi, E. Finazzi, C. Di Valentin, G. Pacchioni, The nature of defects in fluorine-doped TiO_2, J. Phys. Chem. C 112 (2008) 8951-8956.

[56] P. L. W. Tregenna-Piggott, S. P. Best, M. C. M. O'Brien, K. S. Knight, J. B. Forsyth, J. R. Pilbrow, Cooperative Jahn-Teller effect in titanium alum, J. Am. Chem. Soc. 119 (1997), 3324–3332.

[57]P. L. W. Tregenna-Piggott, C. J. Noble, J. R. Pilbrow, The study of the influence of Jahn-Teller coupling and low symmetry strain on the anomalous electron paramagnetic resonance spectrum of titanium(III) doped $CsAl(SO_4)_2{\cdot}12H_2O$, J. Chem. Phys. 113 (2000) 3289-3301.

[58]R. Ameis, S. Kremer, D. Reinen, Jahn-Teller effect of titanium(3+) in octahedral coordination: a spectroscopic study of hexachlorotitanate ($TiCl_6^{3-}$) complexes, Inorg. Chem. 24 (1985) 2751–2754.

[59]G. Corradi, I. M. Zaritskii, A. Hofstaetter, K. Polgár, L. G. Rakitina, Ti^{3+} on Nb site: A paramagnetic Jahn-Teller center in vacuum-reduced $LiNbO_3$:Mg:Ti single crystals, Phys. Rev. B 58 (1998) 8329-8337.

[60] P. Höfer, A. Grupp, H. Nebenführ, M. Mehring, Hyperfine sublevel correlation (hyscore) spectroscopy: a 2D ESR investigation of the squaric acid radical, Chem. Phys. Lett. 132 (1986) 279-282.

[61]I. W. C. E. Arends, R. A. Sheldon, M. Wallau, U. Schuchardt, Oxidative transformations of organic compounds mediated by redox molecular sieves, Angew. Chem. Int. Ed. Engl. 36 (1997) 1144-1163.

[62]R. D. Oldroyd, G. Sankar, J. M. Thomas, D. Ozkaya, Enhancing the performance of a supported titanium epoxidation catalyst by modifying the active center, J. Phys. Chem. B 102 (1998) 1849-1855.

[63]P. T. Tanev, M. Chibwe, T. J. Pinnavaia, Titanium-containing mesoporous molecular sieves for catalytic oxidation of aromatic compounds, Nature 368 (1994) 321-323.

[64]M. Anpo, J. M. Thomas, Single-site photocatalytic solids for the decomposition of undesirable molecules, Chem. Commun. (2006) 3273-3278.

[65] J. Paterson, M. Potter, E. Gianotti, R. Raja, Engineering active sites for enhancing synergy in heterogeneous catalytic oxidations, Chem. Commun. 47 (2011) 517-519.

[66]A. Corma, M. T. Navarro, J. Pérez Pariente, Synthesis of an ultralarge pore titanium silicate isomorphous to MCM-41 and its application as a catalyst for selective oxidation of hydrocarbons, J. Chem. Soc. Chem. Commun. 2 (1994) 147-148.

[67]R. D. Oldroyd, J. M. Thomas, T. Maschmeyer, P. A. Mac Faul, D. W. Snelgrove, K. U. Ingold, D. D. M. Wayner, The titanium(IV)-catalyzed epoxidation of alkenes by *tert*-alkyl hydroperoxides, Angew. Chem. Int. Ed. Engl. 35 (1996) 2787-2790.

[68]T. Maschmeyer, F. Rey, G. Sankar, J. M. Thomas, Heterogeneous catalysts obtained by grafting metallocene complexes onto mesoporous silica, Nature 378 (1995) 159-162.

[69]E. Gianotti, V. Dellarocca, L. Marchese, G. Martra, S. Coluccia, T. Maschmeyer, NH_3 adsorption on MCM-41 and Ti-grafted MCM-41. FTIR, DR UV–Vis–NIR and photoluminescence studies, Phys. Chem. Chem. Phys. 4 (2002) 6019-6115.

[70]S. T. Wilson, B. M. Lok, C. A. Messina, T. R. Cannan, E. M. Flanigen, Aluminophosphate molecular sieves: a new class of microporous crystalline inorganic solids, J. Am. Chem. Soc. 104 (1982) 1146-1147.

[71]S. O. Lee, R. Raja, K. D. Harris, J. M. Thomas, B. F. G. Johnson, G. Sankar, Mechanistic insights into the conversion of cyclohexene to adipic acid by H_2O_2 in the presence of a TAPO-5 catalyst, Angew. Chem. Int. Ed. 42 (2003) 1520-1561.

[72]D. Aurbach, Y. Gofer, O. Chusid, H. Eshel, On nonaqueous electrochemical behavior of titanium and Ti^{4+} compounds, Electrochim. Acta 52 (2007) 2097-2101.

[73] G. Jeschke, R. Rakhmatullin, A. Schweiger, Sensitivity enhancement by matched microwave pulses in one- and two-dimensional electron spin echo envelope modulation spectroscopy, J. Magn. Reson. 131 (1998) 261-271.

[74] L. Liesum, A. Schweiger, Multiple quantum coherence in HYSCORE spectra, J. Chem. Phys. 114 (2001) 9478-9488.

[75]S. Maurelli, E. Morra, S. Van Doorslaer, V. Busico, M. Chiesa, EPR investigation of $TiCl_3$ dissolved in polar solvents - implications for the understanding of active Ti(III) species in heterogeneous Ziegler–Natta catalysts, Phys. Chem. Chem. Phys. 16 (2014) 19625-19633.

[76] A. Hagfelt, M. Grätzel, Light-induced redox reactions in nanocrystalline systems, Chem. Rev. 95 (1995) 49-68.

[77] J. Schneider, M. Matsuoka, M.Takeuchi, J. Zhang, Y. Horiuchi, M. Anpo, D. W. Bahnemann, Understanding TiO_2 photocatalysis: mechanisms and materials. Chem. Rev. 114 (2014) 9919-9986.

[78] R. Howe, M. Gratzel, EPR observation of trapped electrons in colloidal titanium dioxide, J. Phys. Chem. 89 (1985) 4495-4499.

[79] S. Livraghi, M. Chiesa, M. C. Paganini, E. Giamello, On the nature of reduced states in titanium dioxide as monitored by electron paramagnetic resonance. I: the anatase case, J. Phys. Chem. C 115 (2011) 25413-25421.

[80] J. Biedrzycki, S. Livraghi, E. Giamello, S. Agnoli, G. Granozzi, Fluorine- and niobium-doped TiO_2: chemical and spectroscopic properties of polycrystalline n-type-doped anatase, J. Phys. Chem. C 118 (2014) 8462-8473.

[81] S. Livraghi, M. Rolando, S. Maurelli, M. Chiesa, M. C. Paganini, E. Giamello, Nature of reduced states in titanium dioxide as monitored by electron paramagnetic resonance. II: rutile and brookite cases, J. Phys. Chem. C 118 (2014) 22141-22148.

[82] M. Chiesa, M. C. Paganini, S. Livraghi, E. Giamello, Charge trapping in TiO_2 polymorphs as seen by Electron Paramagnetic Resonance spectroscopy, Phys. Chem. Chem. Phys. 15 (2013) 9435-9447.

[83] N. M. Dimitrijevic, Z. V. Saponjic, B. M. Rabatic, O. G. Poluektov, T. Rajh, Effect of size and shape of nanocrystalline TiO_2 on photogenerated charges. An EPR study, J. Phys. Chem. C 111 (2007) 14597-14601.

[84] S. Livraghi, S. Maurelli, M. C. Paganini, M. Chiesa, E. Giamello, Probing the local environment of Ti^{3+} ions in TiO_2 (rutile) by ^{17}O HYSCORE, Angew. Chem. Int. Ed. 50 (2011) 8038-8040.

[85] M. Chiesa, P. Martino, E. Giamello, C. Di Valentin, A. del Vitto, G. Pacchioni, Local environment of electrons trapped at the MgO surface: spin density on the oxygen ions from ^{17}O hyperfine coupling constants, J. Phys. Chem. B 108 (2004) 11529-11534.

[86] M. Chiesa, E. Giamello, C. Di Valentin, G. Pacchioni, Z. Sojka, S. Van Doorslaer, Nature of the chemical bond between metal atoms and oxide surfaces: new evidences from spin density studies of K atoms on alkaline earth oxides, J. Am. Chem. Soc. 127 (2005) 16935-16944.

[87] N. A. Deskins, M. Dupuis, Intrinsic hole migration rates in TiO_2 from density functional theory, J. Phys. Chem. C 113 (2009) 346-358.

[88] A. Schleife, J. B. Varley, A. Janotti, C.G. Van De Walle, Conductivity and transparency of TiO_2 from first principles, Proceedings of SPIE. The International Society for Optical Engineering 8822 (2013) 882205-882205-9.

[89] P. Krüger, S. Bourgeois, B. Domenichini, H. Magnan, D. Chandesris, P. Le Fevre, A. M. Flank, J. Jupille, L. Floreano, A. Cossaro, A. Verdini A. Morgante, Defect states at the TiO_2(110) surface probed by resonant photoelectron diffraction, Phys. Rev. Lett. 100 (2008) 055501-055501-04.

[90] C. Di Valentin, G. Pacchioni , A. Selloni, Reduced and n-type doped TiO_2: nature of Ti^{3+} species, J. Phys. Chem. C, 113 (2009) 20543-20552.

[91] M. Stetvin, C. Franchini, X. Hao, M. Schmid, A. Janotti, M. Kaltak, C. G. Van de Walle, G. Kresse, U. Diebold, Direct view at excess electrons in TiO_2 rutile and anatase, Phys. Rev. Lett. 113 (2014) 086402-086402-05.